Journal of Colloid and Interface Science 606 (2022) 1823–1832

Contents lists available at ScienceDirect

Journal of Colloid and Interface Science

journal homepage: www.elsevier.com/locate/jcis

Unsupervised bubble calorimetry analysis: Surface tension from isothermal titration calorimetry

Pablo F. Garrido [a,*], Margarida Bastos [b], Adrián Velázquez-Campoy [c,d,e,f,g], Alfredo Amigo [a], Philippe Dumas [h], Ángel Piñeiro [a,*]

[a] Departamento de Fisica de Aplicada, Facultade de Fisica, Universidade de Santiago de Compostela, E-15782 Santiago de Compostela, Spain
[b] CIQ-UP, Departamento de Quimica e Bioquimica, Faculdade de Ciencias da Universidade do Porto, R. Campo Alegre 687, P-4169-007 Porto, Portugal
[c] Institute of Biocomputation and Physics of Complex Systems (BIFI), Joint Units IQFR-CSIC-BIFI, and GBsC-CSIC-BIFI, Universidad de Zaragoza, Zaragoza 50018, Spain
[d] Department of Biochemistry and Molecular and Cell Biology, Universidad de Zaragoza, 50009 Zaragoza, Spain
[e] Aragon Institute for Health Research (IIS Aragon), 50009 Zaragoza, Spain
[f] Biomedical Research Networking Centre for Liver and Digestive Diseases (CIBERehd), 28029 Madrid, Spain
[g] Fundacion ARAID, Government of Aragon, 50018 Zaragoza, Spain
[h] IGBMC, Dept of Integrative Biology, Strasbourg University, F67404 Illkirch CEDEX, France

GRAPHICAL ABSTRACT

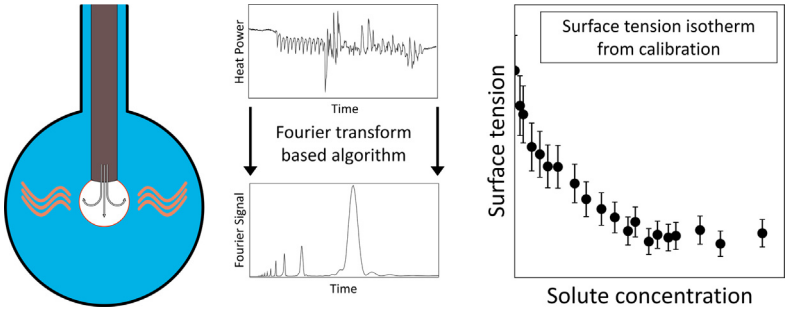

ARTICLE INFO

Article history:
Received 5 July 2021
Revised 13 August 2021
Accepted 14 August 2021
Available online 20 August 2021

Keywords:
Interfaces
Adsorption
Isothermal Titration Calorimetry
Surface Tension
Data analysis

ABSTRACT

Hypothesis: The injection of air into the sample cell of an isothermal titration calorimeter containing a liquid provides a rich-in-information signal, with a periodic contribution arising from the creation, growing and release of bubbles. The identification and analysis of such contributions allow the accurate determination of the surface tension of the target liquid.
Experiments: Air is introduced at a constant rate into the sample cell of the calorimeter containing either a pure liquid or a solution. The resulting calorimetric signal is analyzed by a new algorithm, which is implemented into a computational code.
Findings: The thermal power generated by our experiments is often noisy, thus hiding the periodic signal arising from the bubbles' formation and release. The new algorithm was tested with a range of different types of calorimetric raw data, some of them apparently being just noise. In all cases, the contribution of the bubbles to the signal was isolated and the corresponding period was successfully determined in an automated way. It is also shown that two reference measurements suffice to calibrate the instrument at a given temperature, regardless the injection rate, allowing the direct determination of surface tension values for the liquid contained in the sample cell.

* Corresponding authors.
E-mail addresses: Pablo.Fernandez@usc.es (P.F. Garrido), Angel.Pineiro@usc.es (Á. Piñeiro).

https://doi.org/10.1016/j.jcis.2021.08.115
0021-9797/

1. Introduction

Molecular self-organization in the bulk of a liquid solution is intimately connected to the adsorption at the corresponding liquid-air interface. The surface tension is a property that depends directly on the composition of such interface. Thus, for a solution where the solute molecules do not adsorb , the corresponding surface tension should be undistinguishable from that of the pure solvent. However, the experimental evidence shows that the concentration of a given solute at the border region between a liquid and air can be several orders of magnitude larger than that in the bulk of the denser phase [1]. So, the surface tension can be considered as a highly efficient concentration sensor of a liquid solution. This becomes evident when dissolving hydrophobic or amphiphilic molecules in water as these solutes prefer the air-water interface to the bulk solution, thus leading to a significant decrease of the surface tension until the interface is saturated. At higher concentrations the surface tension becomes practically constant. The onset of this region is known as critical micelle concentration (cmc) or critical aggregation concentration (cac), because micelles of different size and shape, vesicles or other types of aggregates are spontaneously formed in the bulk solution beyond it. The kinetics of these processes plays an important role in how they can be characterized. Small molecules, like typical surfactants, diffuse very quickly and their adsorption can be considered as instantaneous for the observer, while the adsorption of large molecules such as proteins can take several hours [2]. A battery of different methods are available to determine the surface tension of liquid solutions: drop volume, drop profile, capillary rise, maximum bubble pressure or du Noüy ring, among others [3,4], since this is considered a basic property of amphiphilic molecules, with a large number of applications in many industries [5–11].

We have recently proposed a new method to determine surface tension values from Isothermal Titration Calorimetry (ITC) [12] that exhibits clear advantages with respect to other classical alternatives: very low sample consumption, easy automation of the experiments, a rich kinetic signal with meaningful physical information, usefulness for a large range of different solute and solvent molecules, and the possibility of performing experiments for the same system both in the bulk solution and at the interface. This method is based on the injection of air at a constant rate into the sample cell of an ITC instrument, and it can be considered as the first direct application of bubble calorimetry.

The eventual appearance of bubbles in calorimetric cells has traditionally been avoided since they typically introduce significant noise in the measurements. Thus, liquid solutions are often subjected to treatments aimed to remove traces of dissolved air that might perturb the experiments. Here we take advantage of the high sensitivity of modern ITC instruments to register the thermal power resulting from the creation, growing and delivery of relatively small bubbles in different solutions when air is injected in the liquid bulk at a constant rate. The obtained signals have a clear periodic contribution since the size of the bubbles is limited by the surface tension of the liquid contained in the measurement cell. This contribution is often hidden by other significant and more-difficult-to-predict sources of heat such as the coalescence of previously released bubbles in the bulk of the liquid solution, the interaction with the cell walls, temperature fluctuation of the environment, baseline drift due to change of composition in the sample cell, etc. For the experiments using pure water the raw data is extremely clean. The periodic contribution to the signal associated to the formation and delivery of bubbles into the solution, is easy to identify. Additional heat contributions due to the condensation/evaporation of solvent molecules and to the change in heat capacity of the sample cell due liquid displacement upon air injection can also be easily identified in these experiments.

It has been demonstrated that there is a linear correlation between the period of the signal obtained in bubble calorimetry experiments and the surface tension of the liquid contained in the sample cell of the instrument [12]. Thus, upon a suitable calibration, the period can be directly used for surface tension determinations by ITC. For solvents with significant vapor pressure and also for liquid solutions with relatively low surface tension, the signal is especially noisy, and often it is not even possible to identify by eye the periodic contribution arising from the bubbles. This represented a strong barrier for the wide use of this new method. The aim of the present work is to address this issue by developing a protocol able to identify the contribution of the bubbles to the ITC signal for a variety of solvent conditions, as well as to effectively determine the corresponding period in a fully automated way, from which the surface tension can be obtained. Our algorithm was implemented into a computational code and tested using a large variety of thermal power profiles corresponding to measurements of three surfactants in aqueous solution at different concentrations and temperatures, as well as measurements for pure water, ethanol and cyclohexane at the same temperatures. Complementarily, we have optimized our previous protocol for the calibration of the instrument, which is required to provide accurate surface tension values. As a result, it is demonstrated that two single reference measurements suffice to get a transformation factor from the period of the calorimetric bubble signal to the surface tension, regardless the injection rate.

2. Materials and methods

2.1. Materials and sample preparation

Ultrapure water (conductivity of 18.2 MΩ·m, Elix 3 purification system, Milipore Corp.), ethanol (99.8% min. purity from Panreac) and cyclohexane (99.7 % min. purity from Honeywell) were used in the experiments. Octyl-β-D-maltopyranoside (C_8G_2), decyl-β-D-maltopyranoside ($C_{10}G_2$) were purchased from Anatrace, and cetyltrimethylammonium bromide (CTAB) from Sigma-Aldrich. These compounds were used as received, without further purification. All the solutions were degassed trough vacuum prior the ITC measurements. Ethanol, $C_{10}G_2$ and CTAB solutions were prepared directly at their final concentrations. The same process was performed for C_8G_2 except for concentrations below 6 mM, which were prepared by diluting a stock solution at 7.20 mM.

2.2. Surface tension measurements

The surface tension of pure ethanol and $C_{10}G_2$ aqueous solutions at 298 ± 0.1 K, as well as that of water, cyclohexane and C_8G_2 aqueous solutions at 283 ± 0.1 K, 298 ± 0.1 K, 310 ± 0.1 K and 323 ± 0.1 K were measured by using a Lauda drop volume tensiometer (TVT 2 model, Germany) with the measurement cell connected to an external temperature bath. A capillary with inner radius of 1.70 mm and a 2.5 mL syringe were employed in all cases. The measurements were performed using the *standard mode* as programmed in the LAUDA software. In this operation mode, the injection rate is sequentially halved 4 times, registering the maximum volume of the drop when it detaches from the capillary. The initial rates were 0.81 μL/s for water and for the surfactant solutions, and 0.40 μL/s for ethanol and cyclohexane.

2.3. Calorimetric experiments

Three different VP-ITC instruments from MicroCal were employed: ITC-A (version 06.05.673), ITC-B (version 08.01.255)

and ITC-C (version 11.10.994). ITCs A and C are located in the same room while ITC B is in a different laboratory. The experimental procedure was described in our previous work [12]. The employed injection rates (v) range from 0.111 μL/s to 0.022 μL/s and the temperature of both laboratories was 296 ± 2 K. No modifications were applied in any of the ITC commercial instruments. The measurements employed in our previous article on Fluid Interface Calorimetry [12] (ethanol and $C_{10}G_2$ in water solution, both at 298 K and at different injection rates) were recycled here. The rest of the measurements were specifically carried out for the present work.

3. ITC data analysis

Because the raw data corresponding to the injection of air at a constant rate into the sample cell of an ITC instrument is often very noisy, a robust protocol able to effectively analyze a large variety of signals is required. In the present work, air injection measurements were collected for three surfactants in aqueous solution at different concentrations and temperatures, as well as for pure water, ethanol and cyclohexane at the same temperatures. As explained in our previous work, the surface tension of a liquid can be obtained from the period of the signal corresponding to the creation, growing and spontaneous release of bubbles during the air injection experiments [12]. This signal represents one contribution to the thermal power profile in our experiments, but other significant contributions are also present, including the drift in the baseline caused by the change in heat capacity of the sample cell, electrical, mechanical or thermal noise, thermal power caused by the coalescence of bubbles in the sample cell, heat exchange with the environment due to the difference of temperature, amongst other unexpected and/or difficult-to-control phenomena. A selection of raw calorimetric profiles corresponding to different air-injection measurements will be employed to illustrate the different steps of our algorithm. These include a non-trivial but reasonably well-behaved experiment with water (Fig. 1-a, black line), a less ideal experiment with a $C_{10}G_2$ solution (Fig. 1-b, black line), a noisy power profile for a different concentration of the same solution (Fig. 1-c, black line), and a very dirty signal obtained for ethanol (Fig. 1-d, black line). At this point we will ignore the specific sources of the radically different behaviors. The algorithm proposed to get the period of the bubble contribution from the thermal power profile consists in several steps that will be described in detail.

3.1. Baseline correction

There are different methods to obtain characteristic frequencies from a time dependent function with different periodic contributions. The most typical is the application of a Fourier transform. This mapping from the time to the frequency space can be automated in a fully unsupervised way. However, all our measurements contain a drift in the baseline caused by the change in composition of the sample cell upon injection of air into a liquid solution. Approaching this drift, ideally linear, by a series of sinusoidal functions introduces artificial peaks in the resulting Fourier transform. To avoid this problem, a baseline correction is applied to the experimental raw data. A general correction that will be able to address a variety of different behaviors should not be limited to a single function or type of functions. In our case, a series of four sequential filters will be applied to the original signal to get a reasonable baseline. It should be stressed that we are not looking for an accurate baseline that would be required to integrate quantitatively signal perturbations, but for a smooth baseline that prevents the appearance of artificial contributions to the Fourier transform in a subsequent analysis. The filters applied to the raw thermal power profile to reach this aim are: (i) a resolution downgrade; (ii) a Savitzky-Golay filtering protocol; (iii) a moving average; and (iv) an additional Savitzky-Golay filtering for low frequency noise. Finally, the resulting baseline is subtracted from the original data for further analysis.

3.1.1. Resolution downgrade (RD)

The peaks corresponding to the bubble release represent the largest contribution to the periodic signal that we aim to characterize, but they should be ignored for the identification of the baseline. Thus, as a first approach towards this goal, the whole profile is replaced by the average values determined over windows of $\sqrt{10N}$ length, where N is the total number of data points considered. This means that a hypothetical signal described by 1000 points would be distributed in 100 windows, and the whole profile would be replaced by the average of each of these trajectory seg-

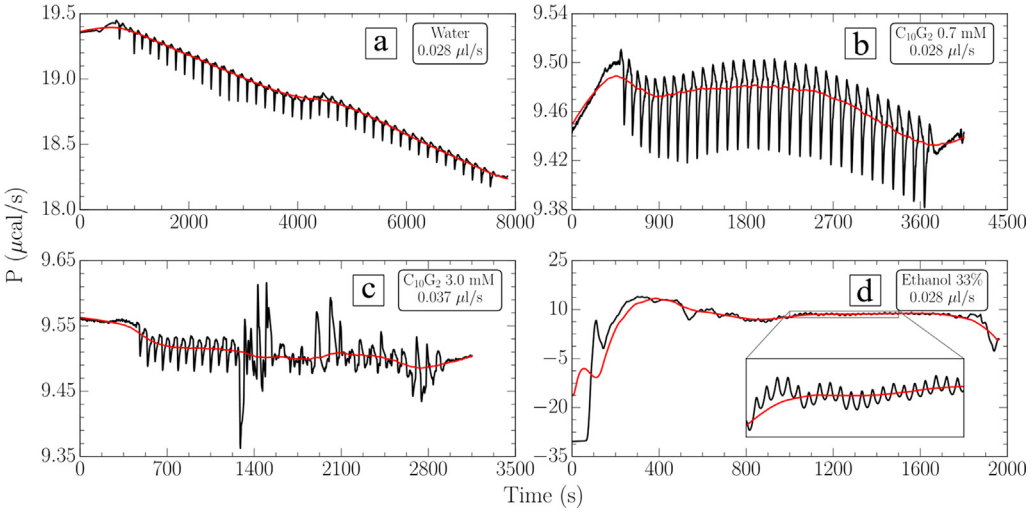

Fig. 1. Black lines: Calorimetric raw data measurements corresponding to four different types of air-injection profiles. In all the cases, air with no specific treatment was injected into the corresponded liquid. The liquid and injection rate of each thermal power profile is indicated in each plot. The inset in the plot corresponding to the ethanol contains a close-up of the signal in the region where the contribution of the bubbles is clearer. Red lines: estimated baselines after the RD followed by SG filtering protocol. (For interpretation of the references to color in this figure legend, the reader is referred to the web version of this article.)

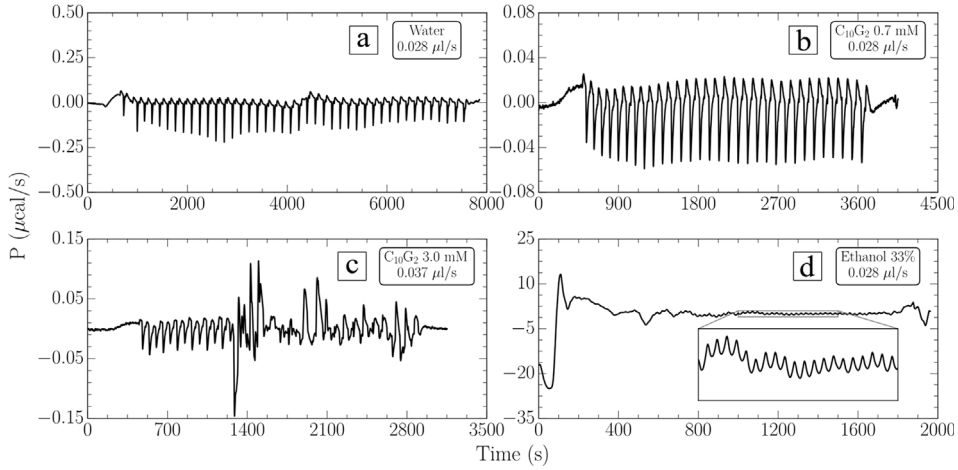

Fig. 2. Same data as in Fig. 1 after baseline subtraction.

ments. The length of the windows was chosen after several trials, considering an adequate result for this filter and taking as a reference the typical criteria used to set the number of bins in histograms. The resulting profile is closer to an ideal baseline than the original raw data, even for the signals with sharp perturbations (Figs. S1 and S2 in the SM).

3.1.2. Savitzky-Golay (SG) filtering

The output of the resolution downgrade is smoothed by applying a SG filtering protocol [13–15] with a second degree fitting polynomial. Due to the heterogeneity of the ITC profiles, we decided to apply four different SG filters using as a window size 10%, 20%, 30% and 40% the length of the downgraded signal in each of them. The average trend obtained from those filters is then filled with the same number of points as the original signal by cubic splines interpolation (Fig. 1).

3.1.3. Moving average (MA)

In order to smooth the high-frequency fluctuations that eventually remain after the previous SG protocol, a moving average was performed, using 10% of the trajectory length as a window size. The impact of this filter is often not significant, but it leads to a less artificial baseline in some cases.

3.1.4. Savitzky-Golay (SG) filter for low frequencies

A single SG filter is finally applied again with a second-degree fitting polynomial and using 50% of the trajectory as a window size. The aim of this filter is to correct low frequency fluctuations. The result of this last filter is only accepted when the difference between the resulting signal and the original data is significantly reduced. An F-test was applied to decide whether or not this filter is applied.

3.1.5. Baseline subtraction

Once the baseline is obtained following the above-described protocol, it is subtracted from the raw data for further analysis (Fig. 2). As it will be shown later, this treatment suffices to prevent the appearance of artificial contributions to the Fast Fourier transform (FFT) caused by the baseline drift.

3.2. Fourier analysis

After removal of the baseline, a Fast Fourier transform (FFT) is applied to get the characteristic frequencies of the signal. The loss of resolution associated to the use of FFT was amended by adding zeros at the end of the trajectory, thus increasing the length of the data array by a factor of 10. This method has been described in detail by Comisarow and Melka [16]. As expected, the application of FFT to the raw data does not provide useful information (Fig. 3, top row). In contrast, the result of the FFT on the baseline-corrected data provides a clear peak that can be associated to the period of the main contribution to the total signal coming from the bubbles, at least for the experiments with less noise and less perturbations in the thermal power profile. This result illustrates the need for the baseline correction on the raw data. However, the application of this filter to the less ideal measurements still shows many peaks, corresponding to artificial contributions of different period (Fig. 3, second row). Thus, we decided to perform a moving FFT (MFFT), similar to a wavelet analysis [17], on the baseline-corrected data in order to isolate the impact of strong perturbations that only affect specific regions of the thermal power profile (Fig. 3, third row). Using this methodology with a window size of 20% of the whole data array, the appearance of local noise along the experiment can be clearly identified. Further to this, an increase in the period for the beginning of the titration experiment is appreciated. However, in some signals the noise or the size of the perturbations is too high and still masks the useful information (Fig. 3, third row). This is due to the different size of the peaks obtained by the FFT in the different regions of the thermal power profile. A local normalization of the area of the spectra obtained from the MFFT was performed to overcome this problem. This strategy clearly improves the signal because the distribution of the spectrum over many peaks, at least for the noisy regions upon normalization of the corresponding area, significantly reduces the height of each peak compared to regions where a single peak results from the local MFFT (Fig. 3, fourth row). This method provides a period that slightly changes along the titration experiment. The final spectrum from which the periods can be directly determined, is obtained from the average of the normalized MFFT (Fig. 3, last row). The whole process, from raw data to final spectrum, is shown in the Supplementary Material (Figs. S1-S10) for 40 different bubble injection experiments.

3.3. Estimation of the period uncertainty

The resolution of the FFT and the uncertainty in the determination of the period are considered the major sources of error. The contribution to the uncertainty coming from the resolution of the FFT, $s_r(T)$, is given by the following equation:

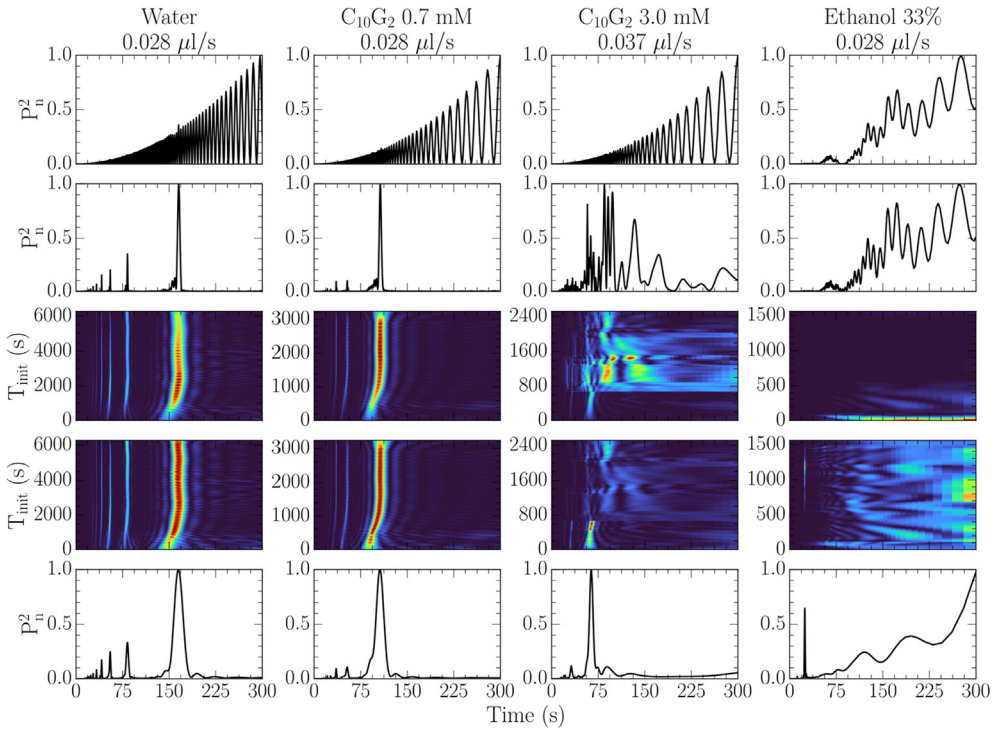

Fig. 3. Illustration of the sequential FFT analyses performed on the thermal power profile obtained from the air titration experiments in the systems indicated on the top of each column. They include: the FFT applied on the raw data (first row), the FFT applied on the baseline-corrected data (second row), the MFFT applied on the baseline-corrected data (third row), the normalized MFFT applied also on the baseline corrected data (fourth row), and the average of the previous normalized MFFT (fifth row). The x-axis is shared for all the plots. The y-axis depends on the plot: for the first, second and fifth rows, it represents the FFT density normalized by the highest peak; for the third and fourth rows, the normalized FFT density is shown with a color gradient (dark blue for lowest values and dark red for highest) and the initial time for each MFFT is represented in the y-axis. (For interpretation of the references to color in this figure legend, the reader is referred to the web version of this article.)

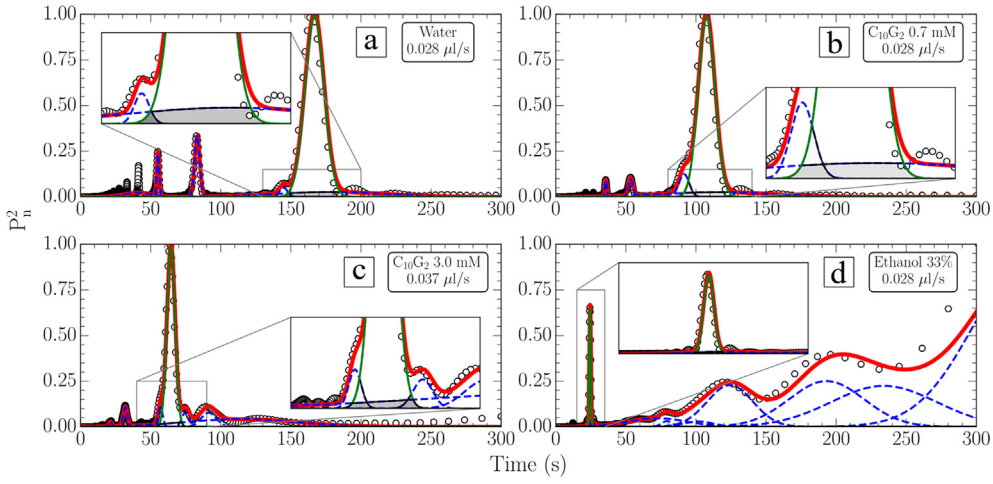

Fig. 4. Fitting of the averaged normalized MFFT spectra corresponding to the same experiments of Fig. 1 to a series of Gaussian functions (red lines) together with the individual Gaussian contributions (blue dashed lines). The green line corresponds to the main peak while the overlapped area is highlighted in grey. For each plot, an inset with a zoom around the overlapping area is shown. (For interpretation of the references to color in this figure legend, the reader is referred to the web version of this article.)

$$s_r(T) = \sqrt{\left(\frac{\partial T}{\partial f}\right)^2 s^2(f)} = \sqrt{T^4 \frac{(\Delta f)^2}{12}} = \frac{1}{\sqrt{12}} T^2 \Delta f \qquad (1)$$

where f is the frequency, $s(f)$ its uncertainty, Δf is the frequency resolution in the transformed space, and T is the period. Eq. (1) is obtained from the standard application of the propagation of uncertainties, considering a square distribution for the frequencies.

The second contribution to the uncertainty comes from the determination of the peak corresponding to the period. The final spectrum, obtained from the average of the normalized MFFT functions, still contains several contributions that were fitted to a series of normal distributions. Gaussian functions were selected for these fittings since they provide a suitable description of the different peaks. The peaks were detected by using the Peakutils Python package [18]. One Gaussian function per peak was employed for the fitting of the spectrum and two additional functions were taken to fit the background. The value of the period can be directly determined from these fittings and the corresponding uncertainty is

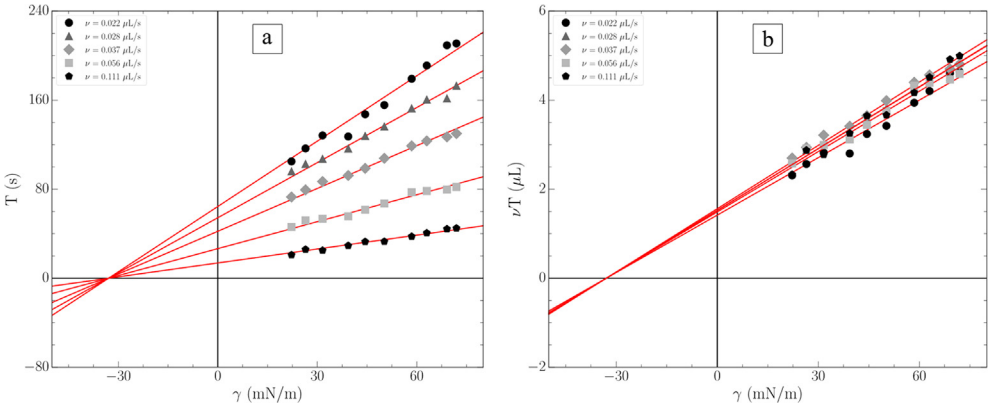

Fig. 5. a: Period obtained from air injection titration experiments by ITC using the protocol described above for different injection rates (see legends), as a function of the experimental surface tension obtained from the literature [19]. b: Bubble volume obtained as the product of the period by the injection rate, as a function of the surface tension for the same systems represented in a. The red lines in both plots represent the linear fittings of the experimental points restrained to share a common point at $\gamma = \gamma_0 = -34.9$ mM/m and T = 0 s. The common value of $p = \nu\, dT/d\gamma$ for all lines is 0.0444 (s(p) = 0.0015). (For interpretation of the references to color in this figure legend, the reader is referred to the web version of this article.)

Table 1
Summary of the experiments performed in the present work, where the employed ITC instruments, injection rates and temperatures are shown.

System	ITC			Injection rate (μl/s)					Temperature (K)			
	A	B	C	0.022	0.028	0.037	0.056	0.111	283	298	310	323
Ethanol-water (1)		x		x	x		x	x		x		
Ethanol-water (2)		x		x	x	x	x	x		x		
$C_{10}G_2$	x		x		x	x	x			x		
C_8G_2	x			x					x	x	x	x
CTAB	x		x		x	x	x			x		

*Ethanol-water solutions were independently prepared and tested twice.

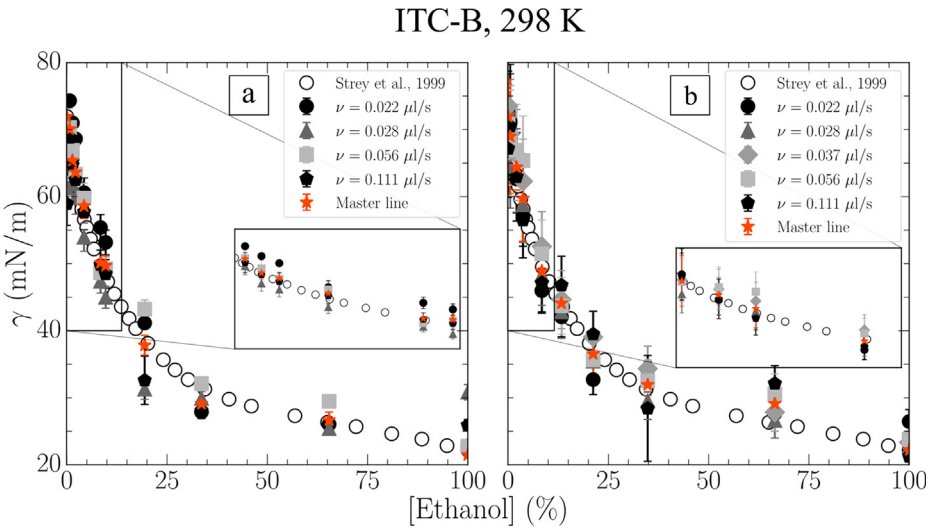

Fig. 6. Comparison between experimental surface tension values of ethanol in water solutions taken from the literature (empty circles) and those obtained following our ITC protocol. Both isotherms have been determined using the same ITC (ITC-B) at the same temperature (298 K). The solutions used for the determination of the isotherms in both plots were independently prepared. Black and grey solid symbols represent the surface tension values obtained from bubble-periods at different concentrations, and calibrations using just pure water and ethanol, at each injection rate. Red symbols represent the surface tension values obtained from the average of all the periods for different injection rates, at each concentration, and using the linear fitting of bubble volume vs surface tension for pure water and ethanol, regardless the injection rate, for the calibration (equivalent to the master line in Fig. 5-b). (For interpretation of the references to color in this figure legend, the reader is referred to the web version of this article.)

obtained from the covariance matrix. For noisy spectra, where more than one curve can be overlapped, the period is obtained from the mean value of all the peaks, weighted by the overlapped area with the main peak, normalized by its own area. This means that the weight for the main peak is 1. The value of the final period (T), its contribution to the uncertainty coming from the fitting and peak overlapping ($s_f(T)$), and the combined total uncertainty ($s_c(T)$) are:

$$T = \frac{\sum_i \tau_i A_i}{\sum_i A_i} \tag{2}$$

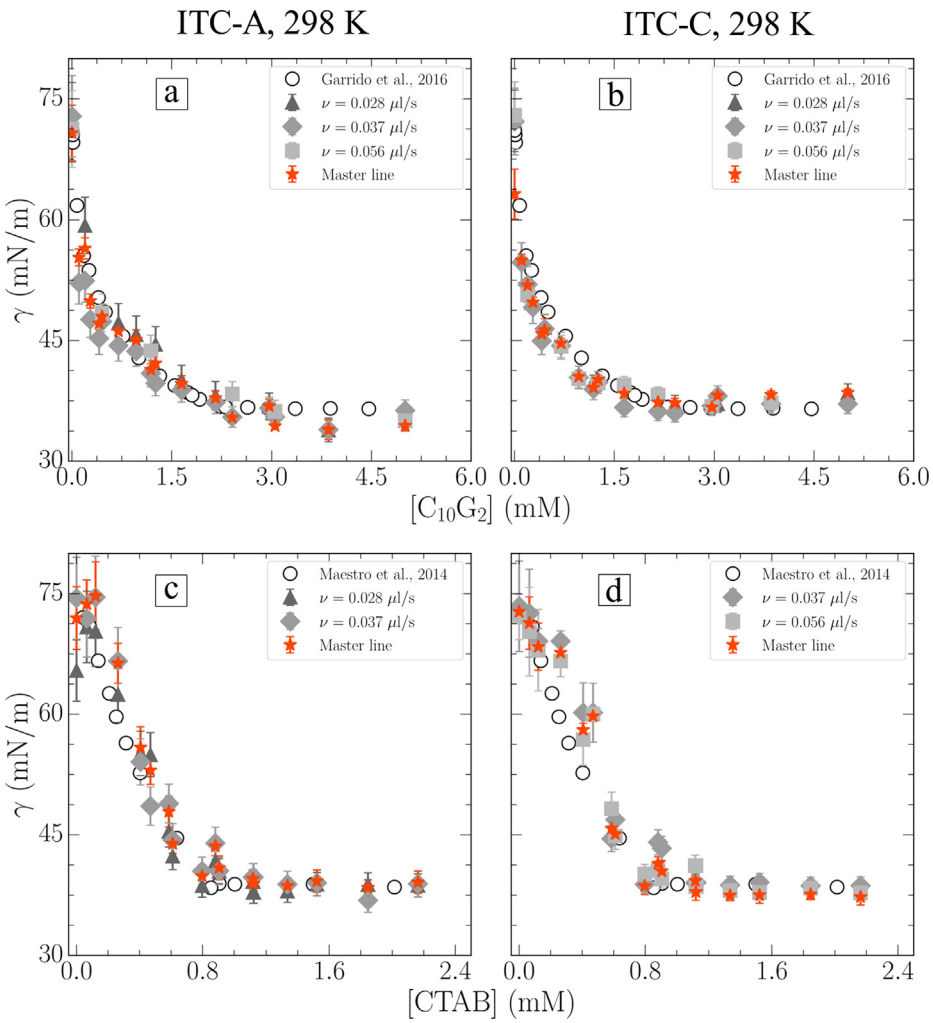

Fig. 7. Comparison between experimental surface tension values of non-ionic surfactant ($C_{10}G_2$) or ionic surfactant (CTAB) aqueous solutions taken from the literature (empty circles) and those obtained following our ITC protocol. For each system, the solutions were prepared once and measured in two different ITCs (ITC-A and ITC-C) at 298 K. Grey solid symbols represent the surface tension values obtained from bubble-periods at different concentrations, and calibrations using just pure water and cyclohexane, at each injection rate. Red symbols represent the surface tension values obtained from the average of all the periods for different injection rates, at each concentration, and using the linear fitting of bubble volume vs surface tension for pure water and cyclohexane, regardless the injection rate, for the calibration (equivalent to the master line in Fig. 5-b). (For interpretation of the references to color in this figure legend, the reader is referred to the web version of this article.)

$$s_f^2(T) = \frac{\sum_i s^2(\tau_i) A_i^2}{\sum_i A_i^2} \tag{3}$$

$$s_c(T) = \sqrt{s_r^2(T) + s_f^2(T)} \tag{4}$$

where τ_i the time value of each fitted peak, $s(\tau_i)$ its uncertainty and A_i the overlapped area normalized with the main peak. The whole process is illustrated in Fig. 4.

3.4. Calibration of the ITC instrument

The volume of a liquid drop pending from a capillary or the maximum pressure of an air bubble injected into a liquid are the observable magnitudes from which the surface tension is typically determined. Quantitative results require a calibration of the corresponding instruments throughout a correlation curve between the measurement and the target property. In our previous work we have observed a linear correlation between the period obtained from air titration experiments and the surface tension of the liquid sample contained in the calorimetric cell. Thus, two different reference compounds suffice to get a calibration curve for a given instrument at each injection rate. Interestingly, we observed that, in all conditions, the extrapolation of the linear correlations between the period and the surface tension at different injection rates converge to a common point with coordinates (γ_0, T = 0) (Fig. 5 and Figs. S11-S12 in the SM). Another observation is that the product p = ν dT/dγ is constant whatever the value of ν within a given experiment, thus leading to a master line in a representation of the bubble volume vs the surface tension that depends mainly on the instrument and on the temperature of the sample cell (Fig. 5 and Figs. S11-S12 in the SM). This means that dV/dγ = p = constant with V = νT is the volume of the bubble reached after the time T. As a result, the two parameters γ_0 and p suffice to characterize completely an experiment like that of Fig. 5. The observed linearity V = V_0 + p γ between the bubble volume and the surface tension is not immediately explained in full from first principles. However, the balance between buoyancy and surface tension when a bubble is about to detach is strictly analogous to the balance between weight and surface tension when a drop of liquid is about to fall in a "drop volume tensiometer". As it is well known the same linearity is observed in the latter situation [3]. Overall, this means that measuring two reference liquids is enough to calibrate the instrument in order to get accurate surface tension measurements

at any injection rate, although the calibration should be periodically repeated if the environmental conditions are not stable.

4. Surface tension validation and reproducibility

Surface tension values for all the systems indicated in the Methods section were measured by ITC, and compared to the values obtained in the present work using a drop volume tensiometer or taken from the literature [19–21]. Surface tension values of water and cyclohexane at different temperatures (Table S1, SM) and ethanol at 298 K (for the ethanol–water system) were employed to calibrate the instruments. These compounds were used for the calibration because they represent extreme cases of well characterized substances with high (water) and low (cyclohexane and ethanol) surface tension values, respectively. Air titration experiments were performed for four different systems as a function of their concentration, for different injection rates and temperatures, using three different ITC instruments, in order to check for instrument reproducibility (see Table 1). The analysis protocol for the determination of the period and the corresponding uncertainty described in the previous section was implemented in a Python code, which was employed to process all the titration thermal power profiles obtained from ITC. Together with the abovementioned libraries, this code is also based on some features from Numpy and Matplotlib [22,23]. These analyses are illustrated for 40 different measurements in the SM (Figs. S1-S10) showing that the algorithm works well for the wide range of trajectories collected for this work. As shown in Figs. 6–8, the surface tension values obtained by ITC agree very well with those obtained from alternative methods. Further to this, the reproducibility when using different injection rates as well as different instruments is good, with discrepancies being in most cases within the calculated uncertainties. Additionally, the effect of the location of the instrument was considered to see if some other parameter such as the external pressure, moisture or different temperature control, could significantly affect the results. Although the noise in the signal or the profile of the raw data can be affected by these external factors, the resulting surface tension values after the previously described analytical treatment are not significantly different.

5. Conclusions and perspectives

Surface tension is one of the most basic properties of liquids and liquid solutions. It is an extraordinary composition sensor, able to detect even nanomolar concentrations of amphiphilic compounds in aqueous solution. Its decrease in the presence of amphiphilic compounds is related to their ability to form aggregates in the bulk [20,24–26]. Equilibrium constants for the formation of complexes between molecules of different surface affinity have even been calculated from surface tension measurements [27]. Many industrial and technological applications are based on the use of amphiphilic compounds with high surface activity. The knowledge of the value

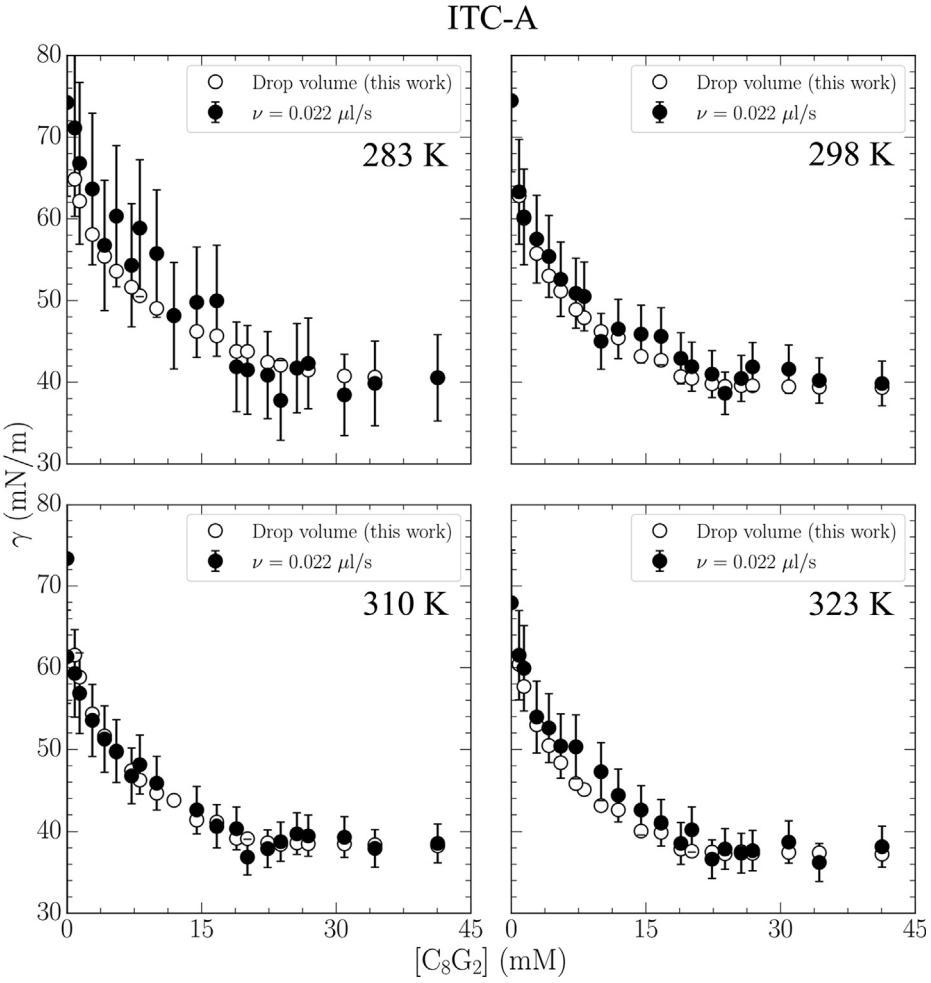

Fig. 8. Comparison between experimental surface tension values of non-ionic surfactant (C_8G_2) aqueous solutions obtained by using a drop volume TVT-2 tensiometer (Lauda) and those obtained following our ITC protocol. All the solutions were prepared once and measured in the same ITC (ITC-A) at 283, 298, 310 and 323 K.

for this property in different conditions and/or concentrations of amphiphiles is key to predict and understand their behavior at molecular level, as well as to optimize or develop new applications. Due to this, a battery of experimental methods is commercially available to measure surface tension of pure liquids and liquid mixtures, such as drop volume, drop profile, capillary rise, maximum bubble pressure, or du Noüy ring, among others [3,4]. Notably, none of these methods is able to simultaneously provide information on the behavior of the studied system in the bulk solution and at the interface. We have recently proposed a new protocol based on the injection of air at a constant rate into the sample cell of an isothermal titration calorimeter that exhibits many advantages with respect to other classical methods of surface tension determination. Bubble calorimetry is the only method that allows measurements of the thermal power associated to different association/dissociation processes both in the bulk and the interface for the same solution, using a small amount of sample, which concentration can be easily changed in a controlled way. This represents a significant saving of time and material. Nevertheless, a problem with these measurements is that they challenge the sensitivity of ITC instruments and so the useful information is often hidden within signal perturbations and noise. The significant breakthrough of the present work is that we propose a general protocol that is able to analyze even the most difficult thermal power profiles in an effective way to assess accurately the periodic nature of the thermal power signal associated with bubble formation and release, which is directly connected to the surface tension of the liquid. This protocol has been implemented into a computational code to allow a fully automated and unsupervised analysis that directly provides surface tension values and the corresponding uncertainties from air titration experiments in an ITC instrument. This computational code is available under request and it is currently being implemented in a freely accessible web application.

6. Contributions

P.F.G. and A.A. performed and analyzed the experiments. Á.P. conceived and supervised the project. P.F.G., M.B., A.V-C., A.A., P. D. and Á.P. analyzed the results and wrote the manuscript.

Declaration of Competing Interest

The authors declare that they have no known competing financial interests or personal relationships that could have appeared to influence the work reported in this paper.

Acknowledgements

The authors thank the financial support of the Spanish Ministry of Economy and Competitiveness (projects MAT2015-71826-P to Á. P. and BFU2016-78232-P to A.V.C.), the Agencia Estatal de Investigación (AEI) (project PID2019-111327GB-I00 to Á. P.) and Fundação para a Ciência e Tecnologia (FCT), Portugal, for CIQUP (project UIDB/00081/2020 to M.B.). P. F. G. thanks the Spanish Ministry of Economy and Competitiveness and the European Social Fund for his predoctoral research grant, reference BES-2016-076761. These research projects were partially supported by European ERDF Funds (MCIU/AEI/FEDER, EU). Facilities provided by the Galician Supercomputing Centre (CESGA) are also acknowledged.

Appendix A. Supplementary material

Supplementary data to this article can be found online at https://doi.org/10.1016/j.jcis.2021.08.115.

References

[1] S.S. Dukhin, G. Kretzschmar, R. Miller, Dynamics of Adsorption at Liquid Interfaces: Theory, Experiment, Application, Elsevier, Amsterdam, 1995.
[2] R. Miller, E.V. Aksenenko, V.S. Alahverdjieva, V.B. Fainerman, C.S. Kotsmar, J. Krägel, M.E. Leser, J. Maldonado-Valderrama, V. Pradines, C. Stefaniu, A. Stocco, R. Wüstneck, Thermodynamics and Kinetics of Mixed Protein/Surfactant Adsorption Layers at Liquid Interfaces, in: J.M. Ruso, Á. Piñeiro (Eds.), Proteins Solut. Interfaces, John Wiley & Sons Inc, Hoboken, NJ, USA, 2013, pp. 389–427, https://doi.org/10.1002/9781118523063.ch20.
[3] H.Y. Erbil, Experimental Determination of Surface Tension at Pure Liquid and Solution Surfaces/Interfaces, in: Surf. Chem. Solid Liq. Interfaces, Blackwell Publishing Ltd., Oxford, UK, 2006: pp. 223–249. https://doi.org/10.1002/9781444305401.ch6.
[4] A.W. Adamson, A.P. Gast, Physical chemistry of surfaces, 6th ed., John Wiley & Sons, New York, 1997.
[5] L.L. Schramm, ed., Surfactants, Cambridge University Press, 2000. https://doi.org/10.1017/CBO9780511524844.
[6] T. Karbowiak, F. Debeaufort, A. Voilley, Importance of surface tension characterization for food, pharmaceutical and packaging products: A review, Crit. Rev. Food Sci. Nutr. 46 (5) (2006) 391–407, https://doi.org/10.1080/10408390591000884.
[7] P. Ragesh, V. Anand Ganesh, S.V. Nair, A.S. Nair, A review on "self-cleaning and multifunctional materials", J. Mater. Chem. A. 2 (36) (2014) 14773–14797, https://doi.org/10.1039/C4TA02542C.
[8] S.B.G.M. O'Brien, Some surface tension and contact angle problems in industry, J. Adhes. Sci. Technol. 6 (9) (1992) 1037–1051, https://doi.org/10.1163/156856192X00926.
[9] N. Mukherjee, B. Bansal, X.D. Chen, Measurement of Surface Tension of Homogenised Milks, Int. J. Food Eng. 1 (2005), https://doi.org/10.2202/1556-3758.1013.
[10] J.M. Luna, R.D. Rufino, L.A. Sarubbo, G.M. Campos-Takaki, Characterisation, surface properties and biological activity of a biosurfactant produced from industrial waste by Candida sphaerica UCP0995 for application in the petroleum industry, Colloids Surfaces B Biointerfaces. 102 (2013) 202–209, https://doi.org/10.1016/j.colsurfb.2012.08.008.
[11] C. Hill, J. Eastoe, Foams: From nature to industry, Adv. Colloid Interface Sci. 247 (2017) 496–513, https://doi.org/10.1016/j.cis.2017.05.013.
[12] P.F. Garrido, M. Bastos, A. Velázquez-Campoy, P. Dumas, Á. Piñeiro, Fluid interface calorimetry, J. Colloid Interface Sci. 596 (2021) 119–129, https://doi.org/10.1016/j.jcis.2021.03.098.
[13] W.H. Press, S.A. Teukolsky, Savitzky-Golay Smoothing Filters, Cit. Comput. Phys. 4 (6) (1990) 669, https://doi.org/10.1063/1.4822961.
[14] A. Savitzky, M.J.E. Golay, Smoothing and differentiation of data by simplified least squares procedures, Anal. Chem. 36 (8) (1964) 1627–1639, https://doi.org/10.1021/ac60214a047.
[15] P. Virtanen, R. Gommers, T.E. Oliphant, M. Haberland, T. Reddy, D. Cournapeau, E. Burovski, P. Peterson, W. Weckesser, J. Bright, S.J. van der Walt, M. Brett, J. Wilson, K.J. Millman, N. Mayorov, A.R.J. Nelson, E. Jones, R. Kern, E. Larson, C.J. Carey, İ. Polat, Y.u. Feng, E.W. Moore, J. VanderPlas, D. Laxalde, J. Perktold, R. Cimrman, I. Henriksen, E.A. Quintero, C.R. Harris, A.M. Archibald, A.H. Ribeiro, F. Pedregosa, P. van Mulbregt, A. Vijaykumar, A.P. Bardelli, A. Rothberg, A. Hilboll, A. Kloeckner, A. Scopatz, A. Lee, A. Rokem, C.N. Woods, C. Fulton, C. Masson, C. Häggström, C. Fitzgerald, D.A. Nicholson, D.R. Hagen, D.V. Pasechnik, E. Olivetti, E. Martin, E. Wieser, F. Silva, F. Lenders, F. Wilhelm, G. Young, G.A. Price, G.-L. Ingold, G.E. Allen, G.R. Lee, H. Audren, I. Probst, J.P. Dietrich, J. Silterra, J.T. Webber, J. Slavič, J. Nothman, J. Buchner, J. Kulick, J.L. Schönberger, J.V. de Miranda Cardoso, J. Reimer, J. Harrington, J.L.C. Rodríguez, J. Nunez-Iglesias, J. Kuczynski, K. Tritz, M. Thoma, M. Newville, M. Kümmerer, M. Bolingbroke, M. Tartre, M. Pak, N.J. Smith, N. Nowaczyk, N. Shebanov, O. Pavlyk, P.A. Brodtkorb, P. Lee, R.T. McGibbon, R. Feldbauer, S. Lewis, S. Tygier, S. Sievert, S. Vigna, S. Peterson, S. More, T. Pudlik, T. Oshima, T.J. Pingel, T.P. Robitaille, T. Spura, T.R. Jones, T. Cera, T. Leslie, T. Zito, T. Krauss, U. Upadhyay, Y.O. Halchenko, Y. Vázquez-Baeza, SciPy 1.0: fundamental algorithms for scientific computing in Python, Nat. Methods. 17 (3) (2020) 261–272, https://doi.org/10.1038/s41592-019-0686-2.
[16] M.B. Comisarow, J.D. Melka, Error Estimates for Finite Zero-Filling in Fourier Transform Spectrometry, Anal. Chem. 51 (13) (1979) 2198–2203, https://doi.org/10.1021/ac50049a032.
[17] G. Kaiser, A Friendly Guide to Wavelets, 1st ed., Birkhäuser Boston (Original work published 1994), Boston, 2011. https://doi.org/10.1007/978-0-8176-8111-1.
[18] L.H. Negri, C. Vestri, lucashn/peakutils: v1.1.0, Zenodo. (2017). https://doi.org/10.5281/ZENODO.887917.
[19] R. Strey, Y. Viisanen, M. Aratono, J.P. Kratohvil, Q.i. Yin, S.E. Friberg, On the Necessity of Using Activities in the Gibbs Equation, J. Phys. Chem. B. 103 (43) (1999) 9112–9116, https://doi.org/10.1021/jp990306w.
[20] P.F. Garrido, P. Brocos, A. Amigo, L. García-Río, J. Gracia-Fadrique, Á. Piñeiro, STAND: Surface Tension for Aggregation Number Determination, Langmuir. 32 (16) (2016) 3917–3925, https://doi.org/10.1021/acs.langmuir.6b0047710.1021/acs.langmuir.6b00477.s001.
[21] A. Maestro, E. Rio, W. Drenckhan, D. Langevin, A. Salonen, Foams stabilised by mixtures of nanoparticles and oppositely charged surfactants: Relationship between bubble shrinkage and foam coarsening, Soft Matter. 10 (36) (2014) 6975–6983, https://doi.org/10.1039/C4SM00047A.

[22] C.R. Harris, K.J. Millman, S.J. van der Walt, R. Gommers, P. Virtanen, D. Cournapeau, E. Wieser, J. Taylor, S. Berg, N.J. Smith, R. Kern, M. Picus, S. Hoyer, M.H. van Kerkwijk, M. Brett, A. Haldane, J.F. del Río, M. Wiebe, P. Peterson, P. Gérard-Marchant, K. Sheppard, T. Reddy, W. Weckesser, H. Abbasi, C. Gohlke, T.E. Oliphant, Array programming with NumPy, Nature. 585 (7825) (2020) 357–362, https://doi.org/10.1038/s41586-020-2649-2.
[23] J.D. Hunter, Matplotlib: A 2D graphics environment, Comput. Sci. Eng. 9 (3) (2007) 90–95, https://doi.org/10.1109/MCSE.2007.55.
[24] H. Wang, H. Kong, J. Zheng, H. Peng, C. Cao, Y. Qi, K. Fang, W. Chen, Systematically exploring molecular aggregation and its impact on surface tension and viscosity in high concentration solutions, Molecules. 25 (2020) 1588, https://doi.org/10.3390/molecules25071588.
[25] C. Hill, A. Czajka, G. Hazell, I. Grillo, S.E. Rogers, M.W.A. Skoda, N. Joslin, J. Payne, J. Eastoe, Surface and bulk properties of surfactants used in fire-fighting, J. Colloid Interface Sci. 530 (2018) 686–694, https://doi.org/10.1016/j.jcis.2018.07.023.
[26] J. Gu, B. Yin, S. Fu, M. Feng, Z. Zhang, H. Dong, F. Gao, Y.S. Zhao, Surface tension driven aggregation of organic nanowires: Via lab in a droplet, Nanoscale. 10 (23) (2018) 11006–11012, https://doi.org/10.1039/C8NR02592D.
[27] Á. Piñeiro, X. Banquy, S. Pérez-Casas, E. Tovar, A. García, A. Villa, A. Amigo, A.E. Mark, M. Costas, On the Characterization of Host−Guest Complexes: Surface Tension, Calorimetry, and Molecular Dynamics of Cyclodextrins with a Non-ionic Surfactant, J. Phys. Chem. B. 111 (2007) 4383–4392, https://doi.org/10.1021/jp0688815.